ACS chemical biology

REVIEW

Molecular Electron Microscopy: State of the Art and Current Challenges

Henning Stahlberg[†] and Thomas Walz[‡,*]

[†]Molecular and Cellular Biology, College of Biological Sciences, University of California at Davis, Briggs Hall, 1 Shields Avenue, Davis, California 95616, and [‡]Department of Cell Biology, Harvard Medical School, 240 Longwood Avenue, Boston, Massachusetts 02115

ABSTRACT The objective of molecular electron microscopy (EM) is to use electron microscopes to visualize the structure of biological molecules. This Review provides a brief overview of the methods used in molecular EM, their respective strengths and successes, and current developments that promise an even more exciting future for molecular EM in the structural investigation of proteins and macromolecular complexes, studied in isolation or in the context of cells and tissues.

*Corresponding author, twalz@hms.harvard.edu.

Received for review February 21, 2008 and accepted April 25, 2008.

Published online May 16, 2008

10.1021/cb800037d CCC: $40.75

Electron microscopy (EM) has been a long-standing tool in the ultrastructural analysis of cells and tissues. Over the last 3 decades, it has also evolved into a powerful technique for the structural study of biological macromolecules. The main difference between this molecular EM and the more conventional EM of fixed tissue sections is its ability to deliver three-dimensional (3D) structures of the studied complexes at the higher resolution necessary to visualize structural details of molecules (on the scale of nanometers) rather than of the gross architecture of cells (on the scale of micrometers). Whereas modern electron microscopes can routinely deliver images of inorganic material at atomic resolution, biological specimens pose great difficulties for EM imaging, significantly reducing the attainable resolution.

Biological specimens consist of up to 80% water, requiring the samples to be prepared in a way that prevents structural collapse upon dehydration in the vacuum of the electron microscope. Biological specimens also consist mainly of light atoms, and the density of proteins is very close to that of vitrified ice (see below), making them low-contrast objects. For thin biological samples, different materials influence mainly the phases of the passing electron beam, not its intensity. To increase image contrast, data are collected out of focus, with the amount of contrast increasing with increasing underfocus. The general effect of defocusing is described, in the weak-phase approximation (*1*), by the so-called contrast transfer function (CTF), a semiperiodic function in reciprocal space (*2*). The main consequences of defocusing are the lack of frequency information around the zero transitions of the CTF in the imaged object, the inversion of phases in some regions of the reciprocal space, and a rapid decrease of the Fourier amplitudes in the high spatial frequency region. Therefore,

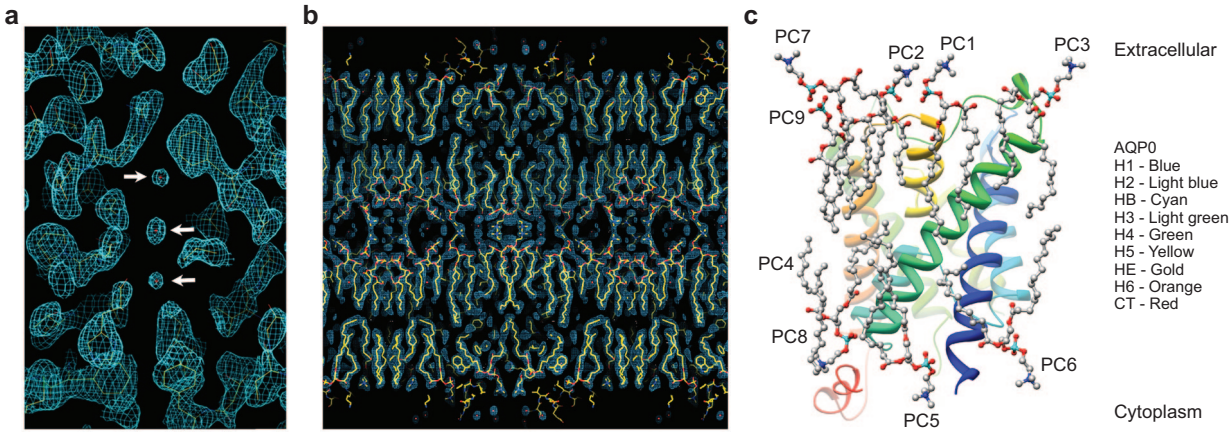

Figure 1. Structure of the AQP0-mediated membrane junction at 1.9 Å resolution obtained by electron crystallography. a) The three water molecules (white arrows) in the water channel of AQP0. b) The two lipid bilayers of the membrane junction with the modeled structures of the lipid molecules. c) Atomic model of an AQP0 subunit with the nine surrounding lipid molecules. Figure adapted from ref 17. Reprinted by permission from Macmillan Publishers Ltd., copyright 2005.

in order to obtain a high-resolution 3D structure, it is necessary to collect data using various, complementary defocus settings and to correct for the effects of the CTF (*3*).

An additional problem is caused by the sensitivity of biological material to electron beam damage, which requires that images have to be recorded with a low electron dose. Such low-dose images unavoidably have a poor signal-to-noise ratio (SNR). Overall, images of biological specimens are dominated by noise, and some information is lost because of the necessity to underfocus the microscope. In effect, it is necessary to develop and apply dedicated digital image processing methods, including alignment, 3D reconstruction, and signal recovery procedures, in order for EM-based structural methods to fulfill their promise.

Initially, biological specimens were prepared for EM by negative staining, a method in which the specimen is dried and embedded in a layer of electron-dense heavy metal salts, which provides high contrast for imaging in the electron microscope. While fast and easy to use, the main disadvantages of negative staining are possible distortions of the molecules resulting from the staining/drying procedure, the low attainable resolution of ~20 Å because of the limited penetrating ability of the stain, and the fact that the image is formed mainly by the stain−protein boundary, so that the structural information is restricted to topographical features of the molecule surface. Distortions of the molecules can be reduced, however, by cryo-negative staining methods (*4*–*6*). For high-resolution reconstructions, vitrification of the unstained specimen in its native buffer solution is the method of choice. In the preparation of cryo-samples, the specimen is rapidly frozen and becomes thus embedded in a layer of vitreous (amorphous) ice (*7, 8*). Although this technique preserves the specimen virtually artifact-free in a near-native environment, images of vitrified specimens are very noisy and have a contrast an order of magnitude lower than that of stained specimens.

Introduction of digital image processing made it possible to determine the 3D structure of biological molecules from very noisy EM images. The computer is used to average images of equivalent molecules to increase the SNR, but improvement of the SNR depends not only on the number of images that are averaged but also on the correct alignment of the images such that the averaging actually improves the signal. In principle, the attained resolution (the minimum size of the structural detail that can be resolved) depends on the number of images averaged, their homogeneity (they should represent the same protein in the same orientation), and the accuracy of alignment; however, in practice the problem is difficult and remains the subject of vigorous research. In addition, the computer is used to combine projection images of the molecule in different orientations to calculate a 3D reconstruction, thus overcoming the problem that electron microscopes can only record 2D

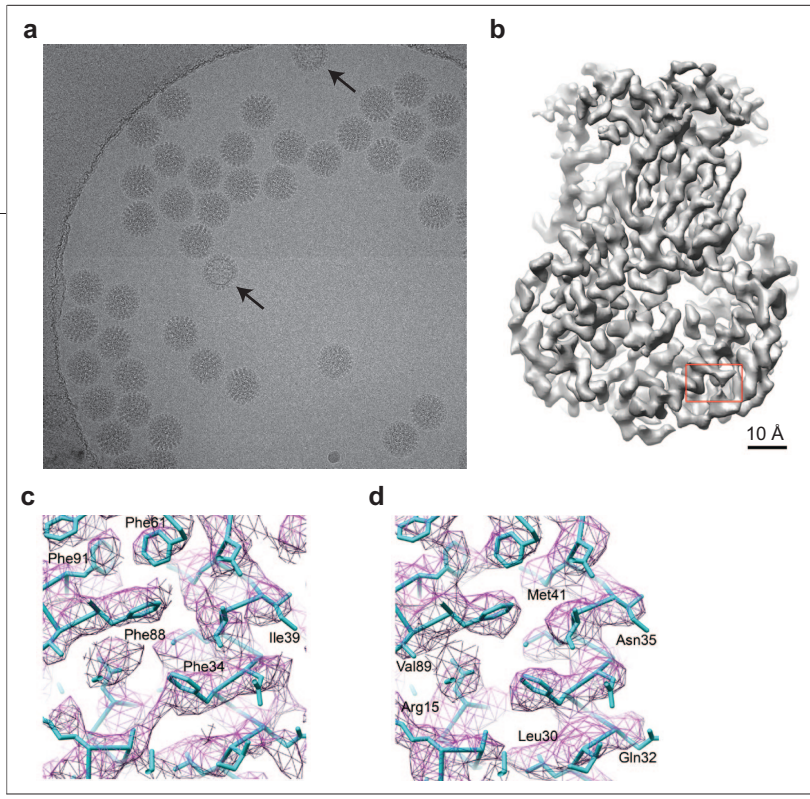

Figure 2. Single-particle EM of the rotavirus inner capsid particle. a) Cryo-EM image of rotavirus inner capsid particles in vitrified ice. The arrows indicate partially damaged particles. b) Overview of the 13-fold averaged viral protein 6 (VP6) trimer at 3.8 Å resolution. The area outlined in red is shown in more detail in panels c and d. c) and d) Density outlined in panel b before (panel c) and after (panel d) 13-fold averaging with the fit crystal structure of VP6 (B. McLain, E. Settembre, R. Bellamy, and S. C. Harrison, unpublished data). Figure adapted from ref 28. Copyright 2008, National Academy of Sciences, U.S.A.

images. Underlying 3D reconstruction are two implicit notions, namely, that electron microscope images are true projections of the imaged molecule and that all images represent identical molecules.

The Methods Used in Molecular EM. Depending on the goal, three distinct approaches can be used in molecular EM to determine the structure of biological molecules: electron crystallography, single-particle EM, and electron tomography.

1. Electron Crystallography. Until very recently, electron crystallography has been the only EM technique that has reached sufficient resolution to produce atomic models of proteins. The method was established by the pioneering work on bacteriorhodopsin (bR) by Unwin and Henderson (*9*), which led to the visualization of the first transmembrane α-helices (*10*) and eventually to the first atomic structure of a membrane protein by electron crystallography (*11*). Electron crystallography is similar to X-ray crystallography (*12*); however, electrons are used to analyze 2D crystals, that is, crystalline arrays of proteins typically just a single molecule thick, rather than X-rays to analyze 3D crystals. The 2D crystals used in electron crystallography are the reason for the high resolution that can be achieved by this technique, because the crystallization accomplishes the alignment of the molecules, which therefore does not need to be done computationally. Thus, the better the order of the 2D crystals, the higher the resolution that can be achieved. Furthermore, in X-ray crystallography, data are only collected in diffraction mode, providing only intensity information and making it necessary to obtain phase information by indirect methods. By contrast, in electron crystallography data can be collected in both diffraction and imaging mode, with the images providing directly all the phase information.

Because electron crystallography uses 2D crystals, it has proven particularly useful in structural studies of membrane proteins (reviewed in ref 13), although it was also used to determine the structure of the αβ tubulin dimer (*14*). Whereas initial electron crystallographic studies focused mostly on naturally occurring 2D crystals, such as purple membranes composed of crystalline bR arrays, work on plant light-harvesting complex II showed that *in vitro* reconstituted 2D crystals can also be sufficiently well ordered to produce atomic models (*15*). Since then, electron crystallography has made major contributions to structural studies of membrane proteins, in particular of aquaporins (reviewed in ref 16). Notably, a recent density map obtained with double-layered 2D crystals of aquaporin-0 at a resolution of 1.9 Å revealed water molecules in the channel of the protein as well as nine lipid molecules surrounding each monomer (Figure 1) (*17*).

2. Single-Particle EM. Although electron crystallography is a very powerful technique, it relies on 2D crystals, which are not always easy to obtain, especially for soluble proteins. The aim of single-particle EM is thus to determine the structure of biological samples from images of individual molecules (single particles). The underlying principle is that a large number (thousands to hundreds of thousands) of molecules in different orientations are imaged, and the images are subsequently computationally aligned and combined to generate a 3D density map (*18*). The ribosome has been, and still is, one of the most prominent specimens used as a test bed for the development of single-particle EM methodology. Continuous advances in instrumentation and image processing algorithms have now allowed the ribosome structure to be determined at subnanometer resolution by single-particle EM (*19, 20*), and for the

first time the fold of an RNA molecule with unknown structure bound to the ribosome could be determined on the basis of its density in the 3D reconstruction (*20*). The number of sub-nanometer-resolution structures is now steadily increasing, for example, GroEL–GroES (*21*), GroEL (*22, 23*), clathrin cages (*24*), and the transferrin–transferrin receptor complex (*25*). The highest-resolution structures have always been obtained with virus capsids because of their icosahedral symmetry; each projection image can be added to the reconstruction in 60 different orientations, greatly simplifying the alignment task and reducing the need for very large numbers of EM images. Thus, with the introduction of CTF correction, the core of the hepatitis B virus became the first single-particle EM reconstruction at subnanometer resolution and the first to visualize α-helices (*26*). Very recently, the first 3D reconstructions of icosahedral particles have been obtained at resolutions that allow building of atomic models into the density maps (*27, 28*), marking another milestone in single-particle EM. To achieve the near-atomic resolution of the density map of the rotavirus inner capsid particle (Figure 2), in addition to the icosahedral symmetry, an additional 13-fold nonicosahedral symmetry was exploited for averaging (*28*).

Producing 3D density maps at ever-increasing resolutions is certainly the goal of single-particle EM; however, unique biological insights can be obtained even from low-resolution projection maps of negatively stained specimens, which revealed, for example, the activation mechanism of integrins (*29*). Low- to intermediate-resolution 3D density maps have provided such a wealth of information on the organization of macromolecular assemblies and the structural changes in proteins and biological complexes associated with their biological functions that it is impossible to name even just the most important examples.

3. Electron Tomography. Electron crystallography and single-particle EM rely on averaging and thus require many identical copies of the same molecule; however, electron tomography can be used to obtain 3D density maps of unique objects *in situ* (*30*). In this approach, the same specimen area is imaged many times at different tilt angles, and the images are computationally combined to generate a density map of the imaged specimen. The recording of electron tomographic tilt series is now fully automated, and tomography has indeed been the technique that pioneered automation in EM data collection.

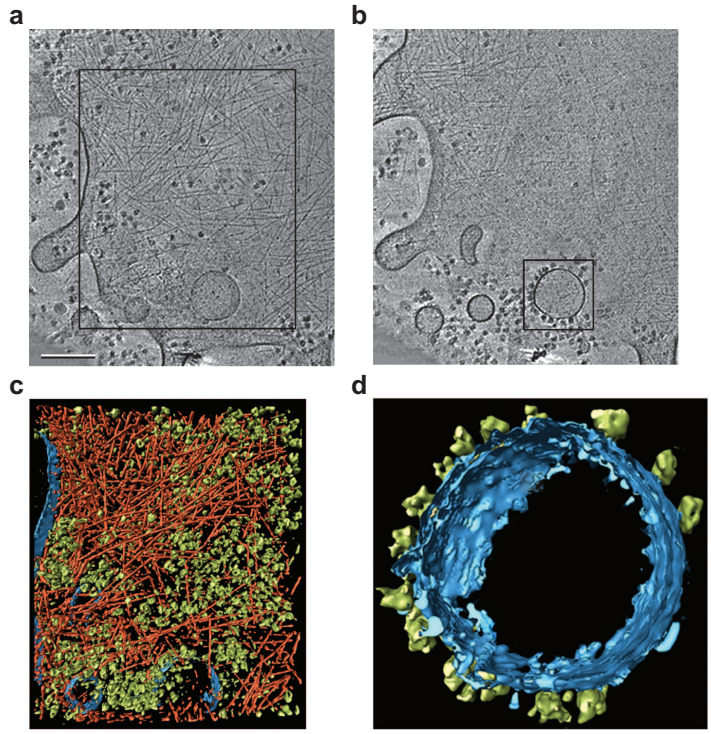

Figure 3. Cryo-electron tomography of a peripheral region of a *Dictyostelium* cell. a) and b) 60 nm thick slices through the electron tomogram. Scale bar is 200 nm. c) Surface rendering of the volume indicated in (b), showing the actin network (red), membranes (blue), and cytoplasmic macromolecular complexes (green). d) Surface rendering of the volume indicated in (b), showing part of the rough endoplasmatic reticulum with ribosome-like densities (green) decorating the membrane (blue). Figure adapted from ref 34. Copyright 2002. Reprinted with permission from AAAS.

The two main limitations of electron tomography are of a physical nature. First, because all images in a tomographic tilt series are collected from the same specimen area, the cumulative dose has to be restricted to the level used in single-particle work to obtain a single image. Hence, the dose used to record an individual image in a tilt series has to be very low. In effect, because there is no averaging, the electron dose limitation forces tomographic reconstructions to be either limited in resolution or to be very noisy. Currently, the resolution of 3D reconstructions of biological, beam-sensitive samples rarely has exceeded 50 Å. Second, the maxi-

mum tilt angle is limited by physical constraints of the stage design of the electron microscope to typically 60° or 70°. The collection of a single-axis tilt series thus means that a wedge-shaped region in Fourier space contains no data, resulting in uncertainties about structural detail in the vertical direction of the reconstructed density map. The missing wedge can be reduced to a missing pyramid by recording dual-tilt axis tilt series, but the requirements for a dual-tilt axis goniometer make this solution technically challenging for most electron microscopes when working with vitrified specimens. Because of the low contrast, the high noise level, and the directional artifacts induced by systematically missing Fourier information, interpretation of electron tomograms is a difficult task. Computer-assisted volume segmentation is used to better understand complex 3D reconstructions. Noise in electron tomograms can be reduced by denoising filters (*e.g.*, refs 31–33), which may, however, also remove fine structural details.

Despite these problems, electron tomography has made stunning progress. In a landmark paper, electron tomography of a vitrified *Dictyostelium* cell revealed the organization of subcellular structures in the filipodium, including the rough endoplasmatic reticulum and the actin cytoskeleton (Figure 3) (*34*). The tomogram also revealed individual proteasomes, demonstrating that the structure of macromolecular complexes can even be determined in their native environment. Other recent successes of electron tomography include the visualization of the architectures of enveloped viruses (*e.g.*, ref 35), nuclear pore complex (*36*), bacterial cytoskeleton (*e.g.*, refs 37 and 38), flagellar motor (*39*), axonemes (*40*), magnetosomes (*41, 42*), and clathrin-coated vesicles (*43*).

KEYWORDS

Molecular electron microscopy: The use of transmission electron microscopy (TEM) to obtain structural information of biological molecules, isolated or in the context of a cell, as opposed to the use of TEM to visualize cellular fine structure.

Cryo-electron microscopy (cryo-EM): The use of TEM to image samples at low temperature. Cryo-EM is typically used in conjunction with vitrified specimens.

Vitrification: The quick-freezing of biological specimens so that they become embedded in a layer of amorphous (or vitrified) ice. Vitreous ice can be maintained at liquid nitrogen temperatures and is a liquid of very high viscosity, comparable to glass.

Electron crystallography: A TEM method used to study the structure of molecules in a two-dimensional array (2D crystal). In materials sciences this method mostly relies on electron diffraction for data collection, while for 2D crystals of biological molecules typically both images and electron diffraction patterns are recorded, which provide phase and amplitude information, respectively.

Current Challenges. Molecular EM has already proved to be immensely useful, yet challenges remain. The following paragraphs provide a brief and certainly incomplete overview of some of the routes that are being taken to realize the full potential of molecular EM.

1. Electron Crystallography. Electron crystallography is a fully developed structure determination technique that is applicable to any protein that forms a 2D array (*44*). Although it can also be used to visualize soluble proteins that form 2D crystals, for instance, on lipid monolayers (*45*), in most cases X-ray crystallography or single-particle EM will be better suited approaches for determining their structure. By contrast, electron crystallography is in principle an excellent approach for determining membrane protein structures, because 2D crystals contain the membrane proteins in a lipid bilayer, their native environment. X-ray crystallography requires the proteins to be arranged in a 3D crystal packing, where extensive protein−protein interactions may alter the native membrane protein conformation. Even though recent progress has been made with 3D crystals of lipid-embedded membrane protein (*46–49*), 3D crystals of membrane proteins usually contain the membrane protein in a detergent micelle, which may further destabilize the native conformation, as was the case for the X-ray structures of the multidrug transporter EmrE (reviewed in ref 50).

So why is it that many more membrane protein structures have been solved by X-ray crystallography? The main reason may lie in the much smaller group of scientists actively engaged in electron crystallography. The small community limits not only the number of membrane proteins that are being studied but also progress in the methodology. While electron crystallography can be used to solve structures, advances are needed in almost every step. Although there are now different ways to produce 2D crystals, based on dialysis (reviewed in refs 51 and 52), dilution (*53*), and detergent chelation (*54*), the mechanisms resulting in highly ordered 2D crystals are not well understood. The process is also often not very reproducible, and commercial screens, such as those available for the growth of 3D crystals, are still lacking for 2D crystallization. A breakthrough in the production of 2D crystals will be required to make electron crystallography a mainstream technique for structure determination and to make it competitive with X-ray crystallography.

Electron crystallographic data collection has improved dramatically since its beginnings. Electron microscopes with helium-cooled top-entry specimen stages, such as the one developed by Fujiyoshi and co-workers

(*55*), and improved specimen preparation methods, such as the carbon sandwich technique (*56*), have especially helped to improve the yield of high-resolution images. Still, specimens suitable for determining a near-atomic structure with currently available data processing software have to be prepared on an extremely flat carbon support film and with the appropriate degree of sugar embedding, drying, and/or freezing (reviewed in ref 57). As ideal preparations are not easily achieved (*58*), preparation of a suitable specimen remains largely a trial-and-error process. Once images and diffraction patterns had been collected, the MRC package (*59*), powerful though not very user-friendly, used to be the only software package to process the data. Only recently have efforts begun to improve and automate electron crystallographic data processing (*60–63*) and to adapt methods commonly used in single-particle EM and X-ray crystallography such as maximum likelihood methods (*64*), molecular replacement (*65, 66*), and phase extension (T.W., unpublished results) to electron crystallography.

2. Single-Particle EM. Although single-particle EM can now produce density maps at subnanometer resolution from images of individual complexes in vitrified ice, the method still suffers from a number of problems. One difficulty is the generation of a reliable first 3D model from the projection images recorded in the electron microscope. Another difficulty concerns the refinement of the initial model to higher resolution, which can be influenced by the noise. Structural heterogeneity may currently be the most severe problem for single-particle EM. If a complex has structural heterogeneity, because of either varying compositions or different conformations, combination of the images into the same 3D reconstruction will result in an incorrect density map. All these problems are further aggravated by the current lack of an objective criterion to assess the accuracy of a reconstructed density map and uncertainties even in determining its resolution. Because a detailed discussion of all the problems is not possible in the confines of this Review, we provide only a brief outline of some of the problems and current efforts to solve them.

2.a. Specimen Preparation. As long as the target protein or complex is stable and can be purified in large amounts, specimen preparation for single-particle EM is straightforward. The situation changes, however, if a complex is not sufficiently abundant or is too labile to be purified even in the low quantities required for single-particle EM. Recently, two new methods have been introduced to address these issues. The GraFix method uses a glycerol gradient to centrifuge the complexes into an increasing concentration of a chemical fixation reagent, thus producing stable complexes for single-particle EM (*67*). In the monolayer purification technique (*68*), a lipid monolayer containing nickel-nitrilotriacetic acid functionalized lipids is cast over a small aliquot of cell lysate containing a His-tagged protein, which can be part of a complex. After a short incubation, the lipid monolayer with the adsorbed proteins can be transferred to an EM grid and used for EM imaging. Because monolayer purification requires only low concentrations of the target complex and eliminates the need for a time-consuming biochemical purification, it is ideally suited for labile and low-abundance complexes. Both methods have not yet been tested extensively and are not likely to always work, stressing the need for further developments of innovative specimen preparation methods for complexes that are labile and/or difficult to purify in large quantities.

2.b. Initial Model Generation. Currently, there are two main approaches to calculate a 3D map from EM images, random conical tilt (RCT) (*69*) and common lines-based methods (*e.g.*, refs 70 and 71). RCT is a robust and reliable 3D reconstruction algorithm that requires recording pairs of images of the same specimen locations under tilted and untilted conditions. It is typically used for specimens prepared by conventional or cryo-negative staining, and the obtained density maps can thus suffer from the artifacts associated with these specimen preparation methods. RCT reconstructions have, however, a defined handedness. Common lines-based reconstruction methods do not require the sample to be imaged under tilted conditions and are usually used to calculate density maps from images of vitrified specimens. Although the im-

KEYWORDS

Single particle electron microscopy: A TEM method to study an ensemble of identical molecules (single particles). While images of the individual particles are noisy, by combining thousands of images the signal-to-noise ratio can be improved and a three-dimensional reconstruction can be calculated.

Electron tomography: A TEM method used to study a single unique specimen by recording a series of images of the same sample area at different tilt angles. By combining the images of the specimen at different tilt angles, the 3D structure of the specimen can be reconstructed.

Docking: Refers to the method of positioning high-resolution structural models of protein subunits into lower-resolution envelopes of protein complexes. The latter can be determined by TEM.

Hybrid methods: The combination of methods that classically addressed different questions using different tools into one hybrid approach that combines the strength of each method. A typical example is the combination of single particle cryo-EM of a complex with X-ray diffraction studies of its subunits and computational modeling of the interactions between the subunits in the complex.

aged molecules are essentially free of preparation artifacts, *ab initio* assignment of orientation parameters to projections is not very robust and can easily lead to incorrect solutions and 3D reconstructions. Because the handedness of common lines-based 3D reconstructions is not defined, it must be determined separately (*72*).

2.c. Refinement. Once an initial model has been produced, the orientation parameters of the particles are refined, for example, by realigning them to reference images calculated from the density map. During this process, the particle images are shifted and rotated to the position where the correlation function between the particle image and a reference is maximal. The newly aligned particle images are combined into a new 3D map, and this refinement process is iterated until a stable reconstruction is obtained. This refinement process fails, however, when a large number of particle images with poor SNR are used, that is, typical cryo-EM data sets of small molecules. The alignment of noisy images to a given reference can be affected by noise correlation with the reference, resulting in an artificial alignment, which prevents the density map from reaching high resolution. At the same time, reference bias on the noise alignment can also lead to artificial, yet reproducible, features and an overestimation of the obtained resolution (*73*). A new function, a weighted correlation coefficient with coherence constraints (*73*), was thus introduced to replace linear, nonweighted cross-correlation, and implemented in the refinement program FREALIGN (*74*). Although the weighted correlation coefficient is less sensitive to signal and may be outperformed by cross-correlation for low-resolution alignment, it is largely independent of noise correlation with the reference and can therefore improve the precision of the high-resolution alignment, resulting in an improved reconstruction. Sigworth has introduced a maximum-likelihood approach to single-particle image processing (*75*), which has since been extended by a classification scheme (*76*). Maximum-likelihood processing is partially based on conventional cross-correlation; however, it does not assign one single correlation-maximized location to each single-particle image. Instead, it determines the reconstruction map that has the highest (maximum) likelihood to correspond to all available experimental particle images. During this process, the maximum-likelihood algorithm considers for each particle a broader range of alignment possibilities, each weighted by a certain profile. This process strongly reduces (but not completely eliminates) the risk of reference noise correlation and therefore is likely to outperform conventional single-particle alignment schemes for noisy data. Maximum-likelihood processing for 3D reconstructions is, however, computationally very expensive, and in the past its use has been limited by the availability of processing resources.

2.d. Resolution Determination. Single particle EM is still lacking an objective resolution determination criterion. Fourier shell correlation (FSC) (*77, 78*), spectral signal-to-noise ratio (SSNR) (*79*), and phase residuals (PR) in resolution ranges (*80, 81*) have all been used to assess the resolution of 3D reconstructions. The most commonly used method is the FSC, in which the data set is split into two randomly assigned subgroups. The particle images from these subgroups are then used to calculate two reconstructions, and the FSC between these two reconstructions is calculated. The resolution can then be defined as the value where the FSC curve falls below a certain threshold, for example, 0.5 (*26*), 0.142 (*72*), or below a certain function (*82*). The FSC is, however, affected by the risk of reference noise correlation, if all noisy particles were aligned to the same reference (*73*). Recently, a new method has been introduced to estimate the resolution of a density map after completion of the image processing. This measure is thus independent of the algorithm that was used to calculate the reconstruction (*83*). Although the method and software tool are not applicable to all data sets, they can provide additional information on the resolution of a 3D reconstruction.

2.e. Model Verification. Two criteria are usually used to assess a 3D reconstruction. A good coverage of the Euler angles of the particles used to calculate the density map indicates that all the views are present that are needed to completely define the structure of the particle. High similarity of the raw images and class averages with reprojections from the density map confirm consistency of the 3D reconstruction with the raw data. These two criteria do not prove, however, that the density map is indeed a faithful representation of the reconstructed molecule. The only reliable way at the moment to judge the accuracy of a single-particle reconstruction is a comparison with available X-ray or NMR structures of the complex or its subunits, but these are not always available. Another way to test the accuracy of a reconstruction has recently been introduced (*72*), which requires that one or a few specimen areas are imaged at

0° as well as at a small tilt angle. If the 3D reconstruction is correct, the orientation parameters of the molecules in the images of tilted and untilted specimens should be consistent with the difference in the tilt angles at which the two images were taken. Nevertheless, an objective measure to assess the accuracy of a single-particle reconstruction, such as R-free in X-ray crystallography, does not exist for single-particle EM and would be highly desirable.

2.f. Heterogeneity. Obtaining a correct 3D reconstruction at subnanometer resolution can be challenging with a homogeneous sample, and a heterogeneous sample multiplies the problems. The reason is that it is usually not straightforward to decide whether two dissimilar images of vitrified particles are images of the same molecule in different orientations or images of the molecule in different conformations. Detection of structural heterogeneity and classification of images of a complex according to its conformational states thus pose currently the greatest hurdles for single-particle EM. Various routes are being taken to deal with heterogeneous specimens. One way is to use RCT of cryo-negatively stained specimens to generate initial 3D maps that can then be used to classify images of vitrified particles (*e.g.*, ref 6). Otherwise, a set of images of vitrified particles can be simultaneously classified and refined into more than one 3D map, an approach currently being implemented in the software package EMAN2 (*84*). A maximum-likelihood approach has also been used for this purpose (*85*). In an alternative approach, all images can be combined in a single 3D reconstruction, which is subjected to a bootstrap 3D variance analysis (*86*). Areas of high variance can then be masked and used for focused classification to produce separate 3D density maps (*87*). Although the various approaches begin to make progress toward handling sample heterogeneity, the problem is far from being solved at this point.

2.g. Hybrid Methods. The most informative use of single-particle reconstructions is the docking of atomic models of individual subunits into the 3D density map of a complex (*88–90*). Even very low resolution density maps obtained with negatively stained specimens can be used for docking, as was done, for example, for complexes of ligands bound to their cell surface receptors (*e.g.*, refs 91 and 92). In this case, the atomic models can simply be placed into the density map to obtain visually the best fit or the fit can be improved by using a real-space structure refinement method (*93*). In either case, the resulting models should not be overinterpreted and should only be seen as a means to obtain an idea of how the individual subunits may be oriented relative to each other, as illustrated by the interferon–receptor complex (Figure 4, panel a) (*91*). With density maps at a resolution of 10 Å or higher, the atomic models can be fit with much higher precision and the positions refined using procedures implemented in software packages used in X-ray crystallography. This was done, for example, to produce pseudoatomic models of the transferrin–transferrin receptor complex (Figure 4, panel b) (*25*) and the D6 barrel clathrin cage (*24*). The resulting models can cautiously be interpreted on the level of individual amino acid residues, but as a rule conclusions should be confirmed by independent means, for example, by mutagenesis. This strategy was employed, for example, to map the receptor binding site on transferrin (*25*).

Docking of atomic models into lower-resolution cryo-EM density maps can be done by domain segmentation and fitting of each domain as a rigid body block into the 3D map. Such docking experiments are, however, subjective, and larger rearrangements of domains often involve tightly coupled motions between smaller regions of the protein, which cannot be traced or understood with the rigid block approach. A flexible docking of atomic structures into a cryo-EM density map can be done by computationally intensive molecular dynamics (MD) simulations or by the computationally easier normal-mode analysis (NMA) (*94, 95*). Normal modes are collaborative oscillations of subunits or regions of a structure that resonate at the same frequency in either identical or opposite phase around a local energy minimum. A multitude of normal modes at different frequencies are usually observed for a complex structure. Conformational transitions of protein structures can often be approximated by superposition of a small subset of the predicted normal modes (*96*). In contrast to MD simulations, NMA ignores the nonharmonic movements of protein domains (*97–99*). In particular, the frequency-limited coarse-grain NMA allows the computationally efficient simulation of the dynamics of large and complex biological systems over longer time scales, but at the cost of sensitivity for finer details like high-frequency side-chain movements (*100*). Large-amplitude low-frequency protein movements, such as those that are induced by ligand binding events or those that have to overcome an energy barrier, however, are strongly non-

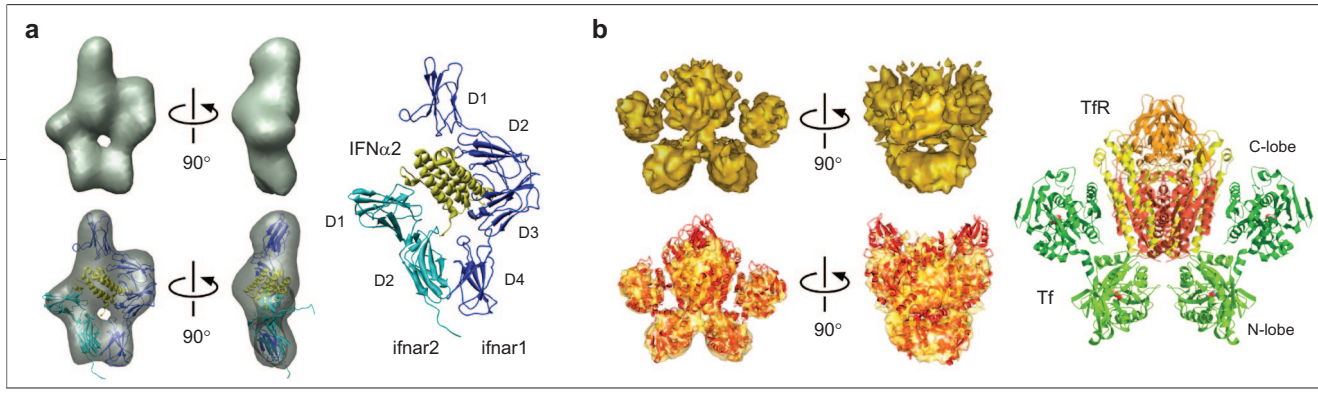

Figure 4. Models of complexes obtained by placing atomic models into single-particle reconstructions. a) Model of an interferon—receptor complex produced by visually placing the atomic models of the subunits into an ~30 Å density map without computational refinement. Such models only provide information on the approximate spatial relationship between the subunits. Figure adapted from ref 91, Copyright 2008. Reprinted with permission from Elsevier. b) Pseudoatomic model of the transferrin—transferrin receptor complex produced by docking atomic models of the subunits into an ~8 Å density map with subsequent computational refinement. The transferrin residues interacting with the receptor were confirmed by mutagenesis. Figure adapted from ref 25, Copyright 2004. Reprinted with permission from Elsevier.

harmonic, so that NMA descriptions may be insufficient in certain cases. Further development is needed to combine the efficiency of an NMA with the sensitivity of full-atom MD simulations. Hybrid methods that combine cryo-EM data with other methods like SAXS and FRET as boundary data for NMA and MD calculations promise to give further insight into protein dynamics (*99*).

3. Electron Tomography. In electron crystallography and single-particle EM, each specimen area is exposed only once, and 3D reconstructions at near-atomic resolution can be obtained by extensive averaging of images of many thousands of identical particles. By contrast, electron tomography is applied to unique objects, precluding averaging and requiring the object to be imaged at many different tilt angles. The damage to the specimen because of the accumulated electron dose resulting from the many exposures puts a physical limit to the resolution that can be obtained by electron tomography. With current sample preparation and imaging methods, it is thus unlikely that the resolution of tomograms of beam-sensitive unique specimens will ever extend much beyond 20 Å, and currently there is not even a measure that could be used to assess the resolution of a tomographic reconstruction. The highest resolutions can be achieved when molecules within a tomogram can be averaged, but this requires proper handling of the missing wedge, which would otherwise interfere with the alignment of the 3D volumes to each other. While various ways have been developed to overcome the missing wedge problem (*e.g.*, ref 101), procedures that fully account for the missing wedge are still missing. Another physical limitation is imposed on tomography by the current design of specimen holders, which only allow the specimen to be imaged to a tilt angle of ~70°. Although design ideas exist that may eventually allow researchers to collect data through a full 180° rotation (*e.g.*, ref 102), the realization of such specimen holders does not seem to be near.

The strength of electron tomography is, however, not obtaining structural information of molecules at high resolution but the possibility to image them in their native environment, entire cells or even tissues. Only a few cells are small enough that they can be directly imaged in the electron microscope (*e.g.*, refs 37 and 103). Most specimens have to be sectioned. To minimize preparation artifacts, traditional chemical fixation can be avoided by cryo-fixation and subsequent freeze-substitution to replace the ice by a resin for subsequent sectioning (*104, 105*). The least artifacts are introduced, however, by freezing the specimen and preparing sections of the frozen specimen that can then be imaged by cryo-EM (*106*). Preparing thin cryo-sections is a daunting task, but a new technology, the thinning of frozen sections using a focused ion beam, may make this task easier in the future (*107*). Methods are now also being developed to first identify an interesting specimen area by light microscopy, before collecting a tilt series of it in the electron microscope (*108, 109*).

Once a tomogram has been calculated, interpretation of the 3D volume can be difficult due to the high noise level and limited resolution of tomograms and the distortions introduced by the missing wedge. Segmentation of the 3D volume is often done interactively, but much work is dedicated to developing automatic procedures (*110, 111*). Identifying molecules of interest in a tomogram presents another challenge. In favorable cases, large macromolecular assemblies can be recognized by their distinctive shape, such as the 26S proteasome and actin filaments, which could be clearly seen in a tomogram of a *Dictyostelium* filopodium (*34*). Efforts are now underway to use 3D maps of macromolecular complexes for computational localization of complexes in tomograms by pattern recognition (*112, 113*). How-

ever, the interiors of cells are very densely packed with proteins and complexes, which may make it difficult to find the boundaries between them in tomographic volumes. The extent by which this "crowding" (*114*) will complicate the interpretation of tomograms is not clear yet. Labeling is an alternative way to identify molecules in tomograms, which will be especially important for the localization of smaller complexes and individual proteins. Labels for electron tomographic studies have to be introduced before the specimen is prepared for EM imaging and they have to be very electron dense to be visible in the tomograms. Labels analogous to the green fluorescence protein, which revolutionized light microscopy (*115*), are thus needed for electron tomography and first attempts to generate a clonable gold label for EM are now underway (*116*).

4. Impact of Instrumentation. Much of past and future progress in molecular EM hinges on developments in instrumentation. Automation of specimen vitrification by the FEI Vitrobot has made it possible for the nonexperienced user to obtain, within a short time, usable cryo-EM grids for single-particle EM and electron tomography (*117*).

Advancements in transmission electron microscopes have mostly been driven by the materials sciences. The introduction of highly coherent and bright field emission gun (FEG) electron sources made it possible to record highly defocused images with only a limited loss in resolution. Because a higher defocus boosts image contrast, FEG instruments have been crucial for obtaining higher resolution structures of biological specimens with their weak-phase-object characteristics. More stable EM electronics and specimen stages allowed for longer exposure times, which is beneficial for the coherence of the illumination and may result in lower beam-damage per dose (*118*). In an alternative approach, dynamic TEM (DTEM) uses ultrashort (up to femtoseconds) electron pulses of variable time duration in either single-shot or stroboscopic imaging mode (*119, 120*). The usefulness of DTEM imaging for biological samples is still unknown. Yet, beneficial effects of DTEM illumination on the consequences of beam damage, sample charging, or specimen movement are conceivable (*121*).

Charge-coupled-device (CCD) cameras revolutionized imaging because they allow images to be captured in digital format, avoiding the time-consuming processes of developing and scanning photographic film. Initial CCD cameras had small imaging areas (typically 1K × 1K chips); recently the first camera with an 8K × 8K chip was introduced. Better data collection strategies are still being developed, including an electron decelerator to improve the imaging characteristics of CCD cameras for fast (high-voltage) electrons (Kenneth Downing, personal communication) and new recording devices, such as imaging plates (*122*) and CMOS detectors (*123, 124*). Together with higher acceleration voltages, energy filters made it possible to image thicker specimens and thus became essential for electron tomography (*125*). Operated in the so-called zero-loss mode, the energy filter removes inelastically scattered electrons, which are responsible for much of the noise in electron micrographs, thus improving the SNR of images, and also of electron diffraction patterns (*126*).

Unstained biological samples are weak phase objects and thus create little image contrast. As discussed above, the current way to enhance contrast is to take images at high defocus, but an alternative way is to use a phase-shifting device. Similar to the effect of a Zernike phase plate for light microscopy (*127, 128*), the phase-shifted electrons then produce strong phase contrast when they recombine with the non-phase-shifted electrons in the image-recording medium. Such phase plates are currently under development, but the various designs still need to overcome significant technical challenges to become of practical use (*129–131*). In another development, aberration-corrected electron lenses have allowed material scientists to record much higher resolution images. Instruments free of spherical aberration have a clean transfer of features to a very high resolution, but the concomitant loss of contrast for the low-resolution frequencies makes this innovation less useful for biological samples with their low inherent contrast (*132*). The combination of an aberration-corrected imaging system with a phase-shifting device could, however, deliver an instrument with strong contrast and high-resolution transfer characteristics. However, even when combined with a phase-shifting device, the low tolerance of focus variations for an aberration-corrected lens system may prevent its use for imaging large, tilted samples—a problem could potentially be addressed by using "spot scan" imaging with dynamic focus adjustment (*133*). At least for untilted biological samples, an electron optical imaging system that combines lenses corrected for spherical and also chromatic aberration (*134*) with a phase-shifting device, may deliver images of biological specimens of unprecedented quality, po-

tentially revolutionizing molecular EM as we know it today.

CONCLUSIONS

EM has already been developed into an extraordinarily versatile tool to obtain structural information of biological molecules that cannot be obtained with any other technique. Yet the potential of molecular EM is even greater, and with the ongoing efforts to improve instrumentation, specimen preparation, data collection, and data processing, the future of molecular EM promises to be truly exciting.

Acknowledgment: Molecular EM work in the Walz laboratory is supported by National Institutes of Health (NIH) Grants R01 EY015107 (to T.W.), RO1 GM082927 (to T.W.), and P01 GM062580 (to S. C. Harrison). Work in the Stahlberg laboratory is supported by NIH Grants R01 GM081653 (to H.S.) and U54 GM074929 (to R. M. Stroud) and National Science Foundation Grant MCB 0447860 (to H.S.).

REFERENCES

1. Wade, R. H. (1992) A brief look at imaging and contrast transfer, *Ultramicroscopy 46*, 145–156.
2. Scherzer, O. (1948) The theoretical resolution limit of the electron microscope, *Appl. Phys. 20*, 20–29.
3. Zhu, J., Penczek, P. A., Schröder, R., and Frank, J. (1997) Three-dimensional reconstruction with contrast transfer function correction from energy-filtered cryoelectron micrographs: procedure and application to the 70S *Escherichia coli* ribosome, *J. Struct. Biol. 118*, 197–219.
4. Adrian, M., Dubochet, J., Fuller, S. D., and Harris, J. R. (1998) Cryo-negative staining, *Micron 29*, 145–160.
5. Golas, M. M., Sander, B., Will, C. L., Lührmann, R., and Stark, H. (2003) Molecular architecture of the multiprotein splicing factor SF3b, *Science 300*, 980–984.
6. Ohi, M., Li, Y., Cheng, Y., and Walz, T. (2004) Negative staining and image classification—powerful tools in modern electron microscopy, *Biol. Proced. Online 6*, 23–34.
7. Adrian, M., Dubochet, J., Lepault, J., and McDowall, A. W. (1984) Cryo-electron microscopy of viruses, *Nature 308*, 32–36.
8. Dubochet, J., Adrian, M., Chang, J. J., Homo, J. C., Lepault, J., McDowall, A. W., and Schultz, P. (1988) Cryo-electron microscopy of vitrified specimens, *Q. Rev. Biophys. 21*, 129–228.
9. Unwin, P. N., and Henderson, R. (1975) Molecular structure determination by electron microscopy of unstained crystalline specimens, *J. Mol. Biol. 94*, 425–440.
10. Henderson, R., and Unwin, P. N. (1975) Three-dimensional model of purple membrane obtained by electron microscopy, *Nature 257*, 28–32.
11. Henderson, R., Baldwin, J. M., Ceska, T. A., Zemlin, F., Beckmann, E., and Downing, K. H. (1990) Model for the structure of bacteriorhodopsin based on high-resolution electron cryo-microscopy, *J. Mol. Biol. 213*, 899–929.
12. Amos, L. A., Henderson, R., and Unwin, P. N. (1982) Three-dimensional structure determination by electron microscopy of two-dimensional crystals, *Prog. Biophys. Mol. Biol. 39*, 183–231.
13. Hite, R. K., Raunser, S., and Walz, T. (2007) Revival of electron crystallography, *Curr. Opin. Struct. Biol. 17*, 389–395.
14. Nogales, E., Wolf, S. G., and Downing, K. H. (1998) Structure of the αβ tubulin dimer by electron crystallography, *Nature 391*, 199–203.
15. Kühlbrandt, W., Wang, D. N., and Fujiyoshi, Y. (1994) Atomic model of plant light-harvesting complex by electron crystallography, *Nature 367*, 614–621.
16. Gonen, T., and Walz, T. (2006) The structure of aquaporins, *Q. Rev. Biophys. 39*, 361–396.
17. Gonen, T., Cheng, Y., Sliz, P., Hiroaki, Y., Fujiyoshi, Y., Harrison, S. C., and Walz, T. (2005) Lipid-protein interactions in double-layered two-dimensional AQP0 crystals, *Nature 438*, 633–638.
18. Frank, J. (2006) *Three-Dimensional Electron Microscopy of Macromolecular Assemblies*, Oxford University Press, New York.
19. Halic, M., Gartmann, M., Schlenker, O., Mielke, T., Pool, M. R., Sinning, I., and Beckmann, R. (2006) Signal recognition particle receptor exposes the ribosomal translocon binding site, *Science 312*, 745–747.
20. Schüler, M., Connell, S. R., Lescoute, A., Giesebrecht, J., Dabrowski, M., Schroeer, B., Mielke, T., Penczek, P. A., Westhof, E., and Spahn, C. M. (2006) Structure of the ribosome-bound cricket paralysis virus IRES RNA, *Nat. Struct. Mol. Biol. 13*, 1092–1096.
21. Ranson, N. A., Clare, D. K., Farr, G. W., Houldershaw, D., Horwich, A. L., and Saibil, H. R. (2006) Allosteric signaling of ATP hydrolysis in GroEL-GroES complexes, *Nat. Struct. Mol. Biol. 13*, 147–152.
22. Ludtke, S. J., Chen, D. H., Song, J. L., Chuang, D. T., and Chiu, W. (2004) Seeing GroEL at 6 Å resolution by single particle electron cryomicroscopy, *Structure 12*, 1129–1136.
23. Stagg, S. M., Lander, G. C., Pulokas, J., Fellmann, D., Cheng, A., Quispe, J. D., Mallick, S. P., Avila, R. M., Carragher, B., and Potter, C. S. (2006) Automated cryoEM data acquisition and analysis of 284742 particles of GroEL, *J. Struct. Biol. 155*, 470–481.
24. Fotin, A., Cheng, Y., Sliz, P., Grigorieff, N., Harrison, S. C., Kirchhausen, T., and Walz, T. (2004) Molecular model for a complete clathrin lattice from electron cryomicroscopy, *Nature 432*, 573–579.
25. Cheng, Y., Zak, O., Aisen, P., Harrison, S. C., and Walz, T. (2004) Structure of the human transferrin receptor-transferrin complex, *Cell 116*, 565–576.
26. Böttcher, B., Wynne, S. A., and Crowther, R. A. (1997) Determination of the fold of the core protein of hepatitis B virus by electron cryomicroscopy, *Nature 386*, 88–91.
27. Jiang, W., Baker, M. L., Jakana, J., Weigele, P. R., King, J., and Chiu, W. (2008) Backbone structure of the infectious epsilon15 virus capsid revealed by electron cryomicroscopy, *Nature 451*, 1130–1134.
28. Zhang, X., Settembre, E., Xu, C., Dormitzer, P. R., Bellamy, R., Harrison, S. C., and Grigorieff, N. (2008) Near-atomic resolution using electron cryomicroscopy and single-particle reconstruction, *Proc. Natl. Acad. Sci. U.S.A. 105*, 1867–1872.
29. Takagi, J., Petre, B. M., Walz, T., and Springer, T. A. (2002) Global conformational rearrangements in integrin extracellular domains in outside-in and inside-out signaling, *Cell 110*, 599–611.
30. Lučič, V., Förster, F., and Baumeister, W. (2005) Structural studies by electron tomography: from cells to molecules, *Annu. Rev. Biochem. 74*, 833–865.
31. Fernández, J. J., and Li, S. (2003) An improved algorithm for anisotropic nonlinear diffusion for denoising cryo-tomograms, *J. Struct. Biol. 144*, 152–161.
32. Pantelic, R. S., Rothnagel, R., Huang, C. Y., Muller, D., Woolford, D., Landsberg, M. J., McDowall, A., Pailthorpe, B., Young, P. R., Banks, J., Hankamer, B., and Ericksson, G. (2006) The discriminative bilateral filter: an enhanced denoising filter for electron microscopy data, *J. Struct. Biol. 155*, 395–408.

33. Stoschek, A., and Hegerl, R. (1997) Denoising of electron tomographic reconstructions using multiscale transformations, *J. Struct. Biol. 120*, 257–265.
34. Medalia, O., Weber, I., Frangakis, A. S., Nicastro, D., Gerisch, G., and Baumeister, W. (2002) Macromolecular architecture in eukaryotic cells visualized by cryoelectron tomography, *Science 298*, 1209–1213.
35. Grünewald, K., Desai, P., Winkler, D. C., Heymann, J. B., Belnap, D. M., Baumeister, W., and Steven, A. C. (2003) Three-dimensional structure of herpes simplex virus from cryo-electron tomography, *Science 302*, 1396–1398.
36. Beck, M., Lučič, V., Förster, F., Baumeister, W., and Medalia, O. (2007) Snapshots of nuclear pore complexes in action captured by cryo-electron tomography, *Nature 449*, 611–615.
37. Kürner, J., Frangakis, A. S., and Baumeister, W. (2005) Cryo-electron tomography reveals the cytoskeletal structure of *Spiroplasma melliferum*, *Science 307*, 436–438.
38. Li, Z., Trimble, M. J., Brun, Y. V., and Jensen, G. J. (2007) The structure of FtsZ filaments *in vivo* suggests a force-generating role in cell division, *EMBO J. 26*, 4694–4708.
39. Murphy, G. E., Leadbetter, J. R., and Jensen, G. J. (2006) *In situ* structure of the complete *Treponema primitia* flagellar motor, *Nature 442*, 1062–1064.
40. Nicastro, D., Schwartz, C., Pierson, J., Gaudette, R., Porter, M. E., and McIntosh, J. R. (2006) The molecular architecture of axonemes revealed by cryoelectron tomography, *Science 313*, 944–948.
41. Komeili, A., Li, Z., Newman, D. K., and Jensen, G. J. (2006) Magnetosomes are cell membrane invaginations organized by the actin-like protein MamK, *Science 311*, 242–245.
42. Scheffel, A., Gruska, M., Faivre, D., Linaroudis, A., Plitzko, J. M., and Schüler, D. (2006) An acidic protein aligns magnetosomes along a filamentous structure in magnetotactic bacteria, *Nature 440*, 110–114.
43. Cheng, Y., Boll, W., Kirchhausen, T., Harrison, S. C., and Walz, T. (2007) Cryo-electron tomography of clathrin-coated vesicles: structural implications for coat assembly, *J. Mol. Biol. 365*, 892–899.
44. Glaeser, R. M., Downing, K. H., DeRosier, D., Chiu, W., and Frank, J. (2007) *Electron Crystallography of Biological Macromolecules*, Oxford University Press, New York.
45. Dietrich, J., and Vénien-Bryan, C. (2005) *Strategies for Two-Dimensional Crystallization of Proteins Using Lipid Monolayers*, Imperial College Press, London.
46. Cherezov, V., Rosenbaum, D. M., Hanson, M. A., Rasmussen, S. G., Thian, F. S., Kobilka, T. S., Choi, H. J., Kuhn, P., Weis, W. I., Kobilka, B. K., and Stevens, R. C. (2007) High-resolution crystal structure of an engineered human β2-adrenergic G protein-coupled receptor, *Science 318*, 1258–1265.
47. Faham, S., and Bowie, J. U. (2002) Bicelle crystallization: a new method for crystallizing membrane proteins yields a monomeric bacteriorhodopsin structure, *J. Mol. Biol. 316*, 1–6.
48. Long, S. B., Campbell, E. B., and Mackinnon, R. (2005) Crystal structure of a mammalian voltage-dependent Shaker family K^+ channel, *Science 309*, 897–903.
49. Rummel, G., Hardmeyer, A., Widmer, C., Chiu, M. L., Nollert, P., Locher, K. P., Pedruzzi, I. I., Landau, E. M., and Rosenbusch, J. P. (1998) Lipidic cubic phases: new matrices for the three-dimensional crystallization of membrane proteins, *J. Struct. Biol. 121*, 82–91.
50. Tate, C. G. (2006) Comparison of three structures of the multidrug transporter EmrE, *Curr. Opin. Struct. Biol. 16*, 457–464.
51. Jap, B. K., Zulauf, M., Scheybani, T., Hefti, A., Baumeister, W., Aebi, U., and Engel, A. (1992) 2D crystallization: from art to science, *Ultramicroscopy 46*, 45–84.
52. Kühlbrandt, W. (1992) Two-dimensional crystallization of membrane proteins, *Q. Rev. Biophys. 25*, 1–49.
53. Remigy, H. W., Caujolle-Bert, D., Suda, K., Schenk, A., Chami, M., and Engel, A. (2003) Membrane protein reconstitution and crystallization by controlled dilution, *FEBS Lett. 555*, 160–169.
54. Signorell, G. A., Kaufmann, T. C., Kukulski, W., Engel, A., and Remigy, H. W. (2007) Controlled 2D crystallization of membrane proteins using methyl-β-cyclodextrin, *J. Struct. Biol. 157*, 321–328.
55. Fujiyoshi, Y. (1989) High resolution cryo-electron microscopy for biological macromolecules, *J. Electron Microsc. 38*, 97–101.
56. Gyobu, N., Tani, K., Hiroaki, Y., Kamegawa, A., Mitsuoka, K., and Fujiyoshi, Y. (2004) Improved specimen preparation for cryo-electron microscopy using a symmetric carbon sandwich technique, *J. Struct. Biol. 146*, 325–333.
57. Chou, H. T., Evans, J. E., and Stahlberg, H. (2007) Electron crystallography of membrane proteins, *Methods Mol. Biol. 369*, 331–343.
58. Glaeser, R. M. (1992) Specimen flatness of thin crystalline arrays: influence of the substrate, *Ultramicroscopy 46*, 33–43.
59. Crowther, R. A., Henderson, R., and Smith, J. M. (1996) MRC image processing programs, *J. Struct. Biol. 116*, 9–16.
60. Gipson, B., Zeng, X., and Stahlberg, H. (2007) 2dx_merge—data management and merging for 2D crystal images, *J. Struct. Biol. 160*, 375–384.
61. Gipson, B., Zeng, X., Zhang, Z. Y., and Stahlberg, H. (2007) 2dx—user-friendly image processing for 2D crystals, *J. Struct. Biol. 157*, 64–72.
62. Philippsen, A., Schenk, A. D., Signorell, G. A., Mariani, V., Berneche, S., and Engel, A. (2007) Collaborative EM image processing with the IPLT image processing library and toolbox, *J. Struct. Biol. 157*, 28–37.
63. Zeng, X., Gipson, B., Zhang, Z. Y., Renault, L., and Stahlberg, H. (2007) Automatic lattice determination for two-dimensional crystal images, *J. Struct. Biol. 160*, 353–361.
64. Zeng, X., Stahlberg, H., and Grigorieff, N. (2007) A maximum-likelihood approach to two-dimensional crystals, *J. Struct. Biol. 160*, 362–374.
65. Gonen, T., Sliz, P., Kistler, J., Cheng, Y., and Walz, T. (2004) Aquaporin-0 membrane junctions reveal the structure of a closed water pore, *Nature 429*, 193–197.
66. Hiroaki, Y., Tani, K., Kamegawa, A., Gyobu, N., Nishikawa, K., Suzuki, H., Walz, T., Sasaki, S., Mitsuoka, K., Kimura, K., Mizoguchi, A., and Fujiyoshi, Y. (2006) Implications of the aquaporin-4 structure on array formation and cell adhesion, *J. Mol. Biol. 355*, 628–639.
67. Kastner, B., Fischer, N., Golas, M. M., Sander, B., Dube, P., Boehringer, D., Hartmuth, K., Deckert, J., Hauer, F., Wolf, E., Uchtenhagen, H., Urlaub, H., Herzog, F., Peters, J. M., Poerschke, D., Lührmann, R., and Stark, H. (2008) GraFix: sample preparation for single-particle electron cryomicroscopy, *Nat. Methods 5*, 53–55.
68. Kelly, D. F., Dukovski, D., and Walz, T. (2008) Monolayer purification: a rapid method for isolating protein complexes for single-particle electron microscopy, *Proc. Natl. Acad. Sci. U.S.A. 105*, 4703–4708.
69. Radermacher, M., Wagenknecht, T., Verschoor, A., and Frank, J. (1987) Three-dimensional reconstruction from a single-exposure, random conical tilt series applied to the 50S ribosomal subunit of Escherichia coli, *J. Microsc. 146*, 113–136.
70. van Heel, M. (1987) Angular reconstitution: a posteriori assignment of projection directions for 3D reconstruction, *Ultramicroscopy 21*, 111–123.
71. Penczek, P. A., Zhu, J., and Frank, J. (1996) A common-lines based method for determining orientations for $N > 3$ particle projections simultaneously, *Ultramicroscopy 63*, 205–218.
72. Rosenthal, P. B., and Henderson, R. (2003) Optimal determination of particle orientation, absolute hand, and contrast loss in single-particle electron cryomicroscopy, *J. Mol. Biol. 333*, 721–745.

73. Stewart, A., and Grigorieff, N. (2004) Noise bias in the refinement of structures derived from single particles, *Ultramicroscopy 102*, 67–84.
74. Grigorieff, N. (2007) FREALIGN: high-resolution refinement of single particle structures, *J. Struct. Biol. 157*, 117–125.
75. Sigworth, F. J. (1998) A maximum-likelihood approach to single-particle image refinement, *J. Struct. Biol. 122*, 328–339.
76. Scheres, S. H., Nunez-Ramirez, R., Gomez-Llorente, Y., San Martin, C., Eggermont, P. P., and Carazo, J. M. (2007) Modeling experimental image formation for likelihood-based classification of electron microscopy data, *Structure 15*, 1167–1177.
77. Saxton, W. O., and Baumeister, W. (1982) The correlation averaging of a regularly arranged bacterial cell envelope protein, *J. Microsc. 127*, 127–138.
78. van Heel, M., and Stöffler-Meilicke, M. (1985) Characteristic views of *E. coli* and *B. stearothermophilus* 30S ribosomal subunits in the electron microscope, *EMBO J. 4*, 2389–2395.
79. Unser, M., Sorzano, C. O., Thévenaz, P., Jonič, S., El-Bez, C., De Carlo, S., Conway, J. F., and Trus, B. L. (2005) Spectral signal-to-noise ratio and resolution assessment of 3D reconstructions, *J. Struct. Biol. 149*, 243–255.
80. Frank, J., Verschoor, A., and Boublik, M. (1981) Computer averaging of electron micrographs of 40S ribosomal subunits, *Science 214*, 1353–1355.
81. van Heel, M. (1987) Similarity measures between images, *Ultramicroscopy 21*, 95–100.
82. van Heel, M., and Schatz, M. (2005) Fourier shell correlation threshold criteria, *J. Struct. Biol. 151*, 250–262.
83. Sousa, D., and Grigorieff, N. (2007) *Ab initio* resolution measurement for single particle structures, *J. Struct. Biol. 157*, 201–210.
84. Tang, G., Peng, L., Baldwin, P. R., Mann, D. S., Jiang, W., Rees, I., and Ludtke, S. J. (2007) EMAN2: an extensible image processing suite for electron microscopy, *J. Struct. Biol. 157*, 38–46.
85. Scheres, S. H., Gao, H., Valle, M. T., , H. G., Eggermont, P. P., Frank, J., and Carazo, J. M. (2007) Disentangling conformational states of macromolecules in 3D-EM through likelihood optimization, *Nat. Methods 4*, 27–29.
86. Penczek, P. A., Yang, C., Frank, J., and Spahn, C. M. (2006) Estimation of variance in single-particle reconstruction using the bootstrap technique, *J. Struct. Biol. 154*, 168–183.
87. Penczek, P. A., Frank, J., and Spahn, C. M. (2006) A method of focused classification, based on the bootstrap 3D variance analysis, and its application to EF-G-dependent translocation, *J. Struct. Biol. 154*, 184–194.
88. Nogales, E., and Grigorieff, N. (2001) Molecular machines: putting the pieces together, *J. Cell Biol. 152*, F1–F10.
89. Volkmann, N., and Hanein, D. (2003) Docking of atomic models into reconstructions from electron microscopy, *Methods Enzymol. 374*, 204–225.
90. Topf, M., and Sali, A. (2005) Combining electron microscopy and comparative protein structure modeling, *Curr. Opin. Struct. Biol. 15*, 578–585.
91. Li, Z., Strunk, J. J., Lamken, P., Piehler, J., and Walz, T. (2008) The EM structure of a type I interferon-receptor complex reveals a novel mechanism for cytokine signaling, *J. Mol. Biol. 377*, 715–724.
92. Skiniotis, G., Boulanger, M. J., Garcia, K. C., and Walz, T. (2005) Signaling conformations of the tall cytokine receptor gp130 when in complex with IL-6 and IL-6 receptor, *Nat. Struct. Mol. Biol. 12*, 545–551.
93. Chen, J. Z., Fürst, J., Chapman, M. S., and Grigorieff, N. (2003) Low-resolution structure refinement in electron microscopy, *J. Struct. Biol. 144*, 144–151.
94. Brooks, B., and Karplus, M. (1983) Harmonic dynamics of proteins: normal modes and fluctuations in bovine pancreatic trypsin inhibitor, *Proc. Natl. Acad. Sci. U.S.A. 80*, 6571–6575.
95. Go, N., Noguti, T., and Nishikawa, T. (1983) Dynamics of a small globular protein in terms of low-frequency vibrational modes, *Proc. Natl. Acad. Sci. U.S.A. 80*, 3696–3700.
96. Tama, F., and Sanejouand, Y. H. (2001) Conformational change of proteins arising from normal mode calculations, *Protein Eng. 14*, 1–6.
97. Frank, J. (2001) Ribosomal dynamics explored by cryo-electron microscopy, *Methods 25*, 309–315.
98. Tama, F., Miyashita, O., and Brooks, C. L., 3rd (2004) Flexible multi-scale fitting of atomic structures into low-resolution electron density maps with elastic network normal mode analysis, *J. Mol. Biol. 337*, 985–999.
99. Gorba, C., Miyashita, O., and Tama, F. (2008) Normal-mode flexible fitting of high-resolution structure of biological molecules toward one-dimensional low-resolution data, *Biophys. J. 94*, 1589–1599.
100. Ma, J. (2005) Usefulness and limitations of normal mode analysis in modeling dynamics of biomolecular complexes, *Structure 13*, 373–380.
101. Förster, F., Medalia, O., Zauberman, N., Baumeister, W., and Fass, D. (2005) Retrovirus envelope protein complex structure *in situ* studied by cryo-electron tomography, *Proc. Natl. Acad. Sci. U.S.A. 102*, 4729–4734.
102. Barnard, D. P., Turner, J. N., Frank, J., and McEwen, B. F. (1992) A 360 degrees single-axis tilt stage for the high-voltage electron microscope, *J. Microsc. 167*, 39–48.
103. Henderson, G. P., Gan, L., and Jensen, G. J. (2007) 3-D ultrastructure of *O. tauri*: electron cryotomography of an entire eukaryotic cell, *PLoS ONE 2*, e749.
104. Müller, M., and Moor, H. (1984) Cryofixation of thick specimens by high pressure freezing. In *The Science of Biological Specimen Preparation for Microscopy and Microanalysis*, pp 131—138, AMF, O'Hare, IL.
105. Steinbrecht, R. A., andMüller, M. (1987) Freeze-substitution and freeze drying. In *Cryotechniques in Biological Electron Microscopy* (Steinbrecht, R. A., and Zierold, K., Eds.), pp 149—172, Springer-Verlag, Berlin and Heidelberg.
106. Al-Amoudi, A., Chang, J. J., Leforestier, A., McDowall, A., Salamin, L. M., Norlén, L. P., Richter, K., Blanc, N. S., Studer, D., and Dubochet, J. (2004) Cryo-electron microscopy of vitreous sections, *EMBO J. 23*, 3583–3588.
107. Marko, M., Hsieh, C., Schalek, R., Frank, J., and Mannella, C. A. (2007) Focused-ion-beam thinning of frozen-hydrated biological specimens for cryo-electron microscopy, *Nat. Methods 4*, 215–217.
108. Schwartz, C. L., Sarbash, V. I., Ataullakhanov, F. I., McIntosh, J. R., and Nicastro, D. (2007) Cryo-fluorescence microscopy facilitates correlations between light and cryo-electron microscopy and reduces the rate of photobleaching, *J. Microsc. 227*, 98–109.
109. Sartori, A., Gatz, R., Beck, F., Rigort, A., Baumeister, W., and Plitzko, J. M. (2007) Correlative microscopy: bridging the gap between fluorescence light microscopy and cryo-electron tomography, *J. Struct. Biol. 160*, 135–145.
110. Pantelic, R. S., Ericksson, G., Hamilton, N., and Hankamer, B. (2007) Bilateral edge filter: photometrically weighted, discontinuity based edge detection, *J. Struct. Biol. 160*, 93–102.
111. Sandberg, K. (2007) Methods for image segmentation in cellular tomography, *Methods Cell Biol. 79*, 769–798.
112. Best, C., Nickell, S., and Baumeister, W. (2007) Localization of protein complexes by pattern recognition, *Methods Cell Biol. 79*, 615–638.
113. Robinson, C. V., Sali, A., and Baumeister, W. (2007) The molecular sociology of the cell, *Nature 450*, 973–982.
114. Grünewald, K., Medalia, O., Gross, A., Steven, A. C., and Baumeister, W. (2003) Prospects of electron cryotomography to visualize macromolecular complexes inside cellular compartments: implications of crowding, *Biophys. Chem. 100*, 577–591.

115. Stearns, T. (1995) Green fluorescent protein. The green revolution, *Curr. Biol. 5*, 262–264.
116. Mercogliano, C. P., and DeRosier, D. J. (2007) Concatenated metallothionein as a clonable gold label for electron microscopy, *J. Struct. Biol. 160*, 70–82.
117. Iancu, C. V., Tivol, W. F., Schooler, J. B., Dias, D. P., Henderson, G. P., Murphy, G. E., Wright, E. R., Li, Z., Yu, Z., Briegel, A., Gan, L., He, Y., and Jensen, G. J. (2006) Electron cryotomography sample preparation using the Vitrobot, *Nat. Protoc. 1*, 2813–2819.
118. Chen, J. Z., Sachse, C., Xu, C., Mielke, T., Spahn, C. M., and Grigorieff, N. (2008) A dose-rate effect in single-particle electron microscopy, *J. Struct. Biol. 161*, 92–100.
119. Armstrong, M. R., Boyden, K., Browning, N. D., Campbell, G. H., Colvin, J. D., DeHope, W. J., Frank, A. M., Gibson, D. J., Hartemann, F., Kim, J. S., King, W. E., LaGrange, T. B., Pyke, B. J., Reed, B. W., Shuttlesworth, R. M., Stuart, B. C., and Torralva, B. R. (2007) Practical considerations for high spatial and temporal resolution dynamic transmission electron microscopy, *Ultramicroscopy 107*, 356–367.
120. Lobastov, V. A., Srinivasan, R., and Zewail, A. H. (2005) Four-dimensional ultrafast electron microscopy, *Proc. Natl. Acad. Sci. U.S.A. 102*, 7069–7073.
121. Glaeser, R. M. (2008) Cryo-electron microscopy of biological nanostructures, *Phys. Today 61*, 48–54.
122. Mori, N., Oikawa, T., Katoh, T., Miyahara, J., and Harada, Y. (1988) Application of the "imaging plate" to TEM image recording, *Ultramicroscopy 25*, 195–201.
123. McMullan, G., Cattermole, D. M., Chen, S., Henderson, R., Llopart, X., Summerfield, C., Tlustos, L., and Faruqi, A. R. (2007) Electron imaging with Medipix2 hybrid pixel detector, *Ultramicroscopy 107*, 401–413.
124. Milazzo, A. C., Leblanc, P., Duttweiler, F., Jin, L., Bouwer, J. C., Peltier, S., Ellisman, M., Bieser, F., Matis, H. S., Wieman, H., Denes, P., Kleinfelder, S., and Xuong, N. H. (2005) Active pixel sensor array as a detector for electron microscopy, *Ultramicroscopy 104*, 152–159.
125. Grimm, R., Bärmann, M., Häckl, W., Typke, D., Sackmann, E., and Baumeister, W. (1997) Energy filtered electron tomography of ice-embedded actin and vesicles, *Biophys. J. 72*, 482–489.
126. Yonekura, K., Maki-Yonekura, S., and Namba, K. (2002) Quantitative comparison of zero-loss and conventional electron diffraction from two-dimensional and thin three-dimensional protein crystals, *Biophys. J. 82*, 2784–2797.
127. Zernike, F. (1935) Das Phasenkontrastverfahren bei der mikroskopischen Beobachtung, *Phys. Z. 36*, 848–851.
128. Zernike, F. (1955) How I discovered phase contrast, *Science 121*, 345–349.
129. Cambie, R., Downing, K. H., Typke, D., Glaeser, R. M., and Jin, J. (2007) Design of a microfabricated, two-electrode phase-contrast element suitable for electron microscopy, *Ultramicroscopy 107*, 329–339.
130. Hosokawa, F., Danev, R., Arai, Y., and Nagayama, K. (2005) Transfer doublet and an elaborated phase plate holder for 120 kV electron-phase microscope, *J. Electron Microsc. 54*, 317–324.
131. Majorovits, E., Barton, B., Schultheiss, K., Pérez-Willard, F., Gerthsen, D., and Schröder, R. R. (2007) Optimizing phase contrast in transmission electron microscopy with an electrostatic (Boersch) phase plate, *Ultramicroscopy 107*, 213–226.
132. Evans, J. E., Hetherington, C. J., Kirkland, A. I., Chang, L. Y., Stahlberg, H., and Browning, N. D. (2008) Low-dose aberration corrected cryo-electron microscopy of organic specimens*Ultramicroscopy*.
133. Downing, K. H. (1991) Spot-scan imaging in transmission electron microscopy, *Science 251*, 53–59.
134. Haider, M., Müller, H., Uhlemann, S., Zach, J., Loebau, U., and Hoeschen, R. (2007) Prerequisites for a C(c)/C(s)-corrected ultrahigh-resolution TEM, *Ultramicroscopy 108*, 167–178.